Supporting Information

Photocatalytic Activation and Reduction of CO_2 to CH_4 over Single Phase Nano Cu_3SnS_4: A Combined Experimental and Theoretical Study

Neha Sharma,[#,a] *Tilak Das,*[#,a] *Santosh Kumar,*[b] *Reshma Bhosale**[,a] *Mukul Kabir*[a] *and Satishchandra Ogale**[,a]

[a]Department of Physics and Centre for Energy Science, Indian Institute of Science Education and Research (IISER), Pune, Dr. Homi Bhabha Road, Pune, 411008, India.

[b]Department of Chemical Engineering, University of Bath, Claverton, Bath BA2 7AY, U.K.

[#] Authors have equal contribution.

***Corresponding Authors**

E-mail: reshmabhosale10@gmail.com

E-mail: satishogale@gmail.com, satishogale@iiserpune.ac.in

SI 1: Tauc plot

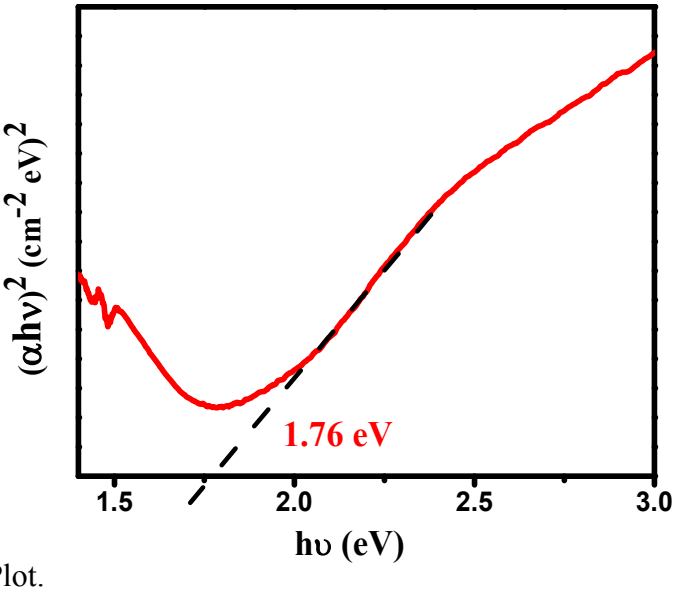

Figure S1: Tauc Plot.

SI 2: Photocatalytic Experiment

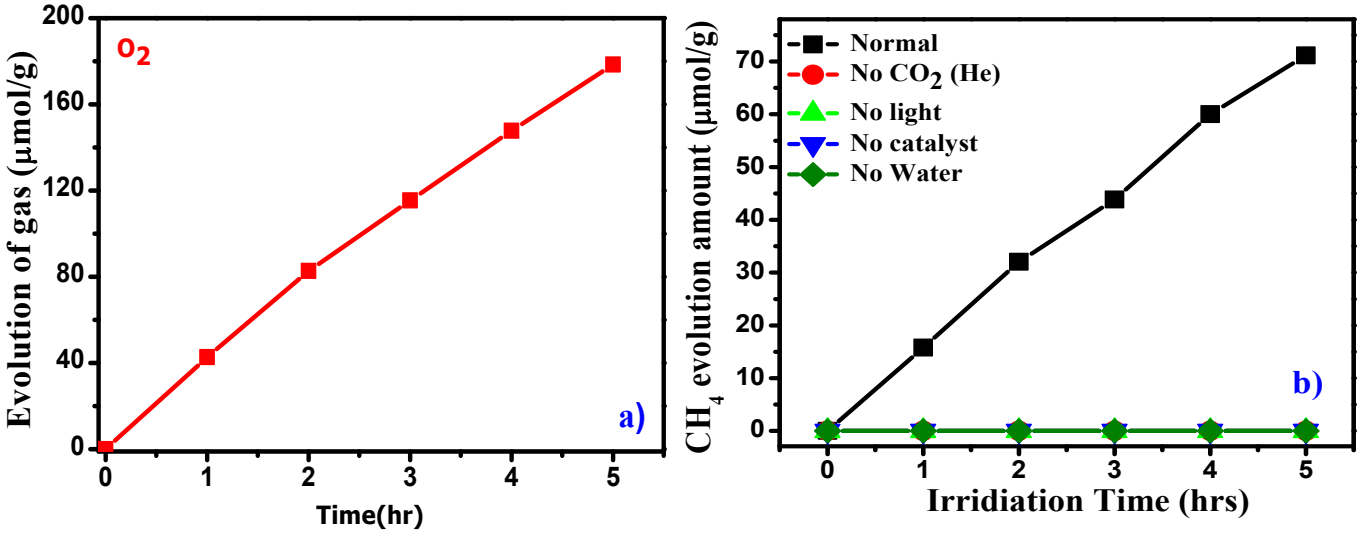

Figure S2: a) O_2 evolution with time **b)** Control experiment of photocatalytic CO_2 reduction over CTS

After 5 hours of amount of gas evolution is given:

1) Amount of CO = 42.4 μmol/g

2) Amount of CH_4 = 71.2 μmol/g

3) Amount of H_2 = 31.4 μmol/g

4) Amount of O_2 = 178.4μmol/g.

Equations involved in photocatalytic reactions:

$CO_2 + 2H^+ + 2e^-$ ------- CO

$CO_2 + 8H^+ + 8e$- ---------- CH_4

$2H+ + 2e^-$ ---------- H_2

$2H_2O + 4h^+$ ---------- $O_2 + 4H^+ + 4e$-

Therefore, as per above equations, electrons are consumed in production of reduced products and each corresponding reduction reaction generates O_2 by consumption of holes. Hence, the evolution of O_2 (178.4 μmol/g) is summation of overall O_2 produced from oxidation reactions. In this respect the stoichiometric ratio of ($CO+H_2$): O_2 is 1:2 and for CH_4: O_2 ratio is 1:2. The calculated O_2 evolved corresponding to CO and H_2 evolution reaction is 73.8 μmol/g where as O_2 evolution corresponding to CH_4 evolution is 142.4 μmol/g. So overall, theoretically calculated evolved O_2 is 179.3 μmol/g. Experimentally by photocatalytic CO_2 reduction over CTS we obtained 178.4 μmol/g which is almost equivalent to theoretically calculated O_2. This indicates that stoichiometrically products are produced and water is consumed as a reducing agent.

S3: Density Functional Theory and Methodology

The crystal structure of the Cu_3SnS_4 (CTS) bulk phases was fully optimized using plane-wave based DFT code Vienna Ab-initio Simulation Package (VASP)[1,2] within the Perdew-Burke-

Ernzerhof (PBE) formulation of the exchange-correlation energy.[3] The core electrons have been approximated with projector augmented wave method (PAW)[3,4] as implemented in VASP pseudopotentials and valence electrons have been treated with plane wave basis set with energy cut-off 650 eV. The valence configuration have been considered carefully with 17 electrons for Cu ($3p^6 3d^{10} 4s^1$), 14 electrons for Sn ($4d^{10}$ $5s^2$ $5p^2$) and 6 electrons for S ($3s^2$ $3p^4$), 6 electrons for O ($2s^2$ $2p^4$), 4 electrons for C ($2s^2$ $2p^2$), and 1 electron for H ($1s^1$) atoms. The energy convergence during the self-consistent cycle using the conjugate gradient algorithm was ensured with convergence threshold criteria 1×10^{-6} eV and force convergence was set to 1×10^{-3} eV/Å. The Monk horst-Pack k-point mesh of size 6 × 8 × 8 sampling was used for structural optimization for bulk phase calculations.[5] The optimized (experimental) lattice parameters of the bulk phase of Cu_3SnS_4 by using PBE-GGA functional are a = 7.585Å (7.530Å), b = 6.568Å (6.604Å) and c = 6.317Å (6.313Å) with almost negligible volume changes (~1%) compared to the known experimental data.

Over the VASP optimized bulk crystal of CTS, the XPS simulation were performed using the full-potential linearized augmented plane-wave plus local orbital code WIEN2K[6] for confirmation of the presence of Cu^{1+} and Cu^{2+} ion types of Cu in the bulk phase (we call them Cu1 and Cu2, now on). The convergence parameters and muffin-tin radii of the elements were chosen by default values and calculated DOS watch matched with PAW PBE-GGA data. A k-mesh size 4 × 4 × 4 was enough to reach convergence for the all XPS simulations of the core-hole over the 2 × 2 × 2 supercell of the bulk structure. In our core-hole calculations, we have explicitly removed one core electron from the target atom and placed in the conduction band. Here, we have only simulated for L_2 edge of the Cu1 and Cu2 atom of CTS and compared with experimental data. And, hence for this purpose the computed data are broadened and shifted according to experimental input.

Experimentally, XPS of S 2p spectrum shows two peaks i.e. $2p_{3/2}$ (162 eV) and $2p_{1/2}$ (163.3 eV) as given in Figure S3a which is indicating S in S^{2-} oxidation state. The spin-orbit doublet of Sn 3d spectrum was observed with two peaks of Sn $3d_{5/2}$ (487.3 eV) and Sn $3d_{3/2}$ (495.6 eV) to be deconvulated into two peaks each (Figure S3b). This indicates that Sn exists in both 2+ and 4+ oxidation states.

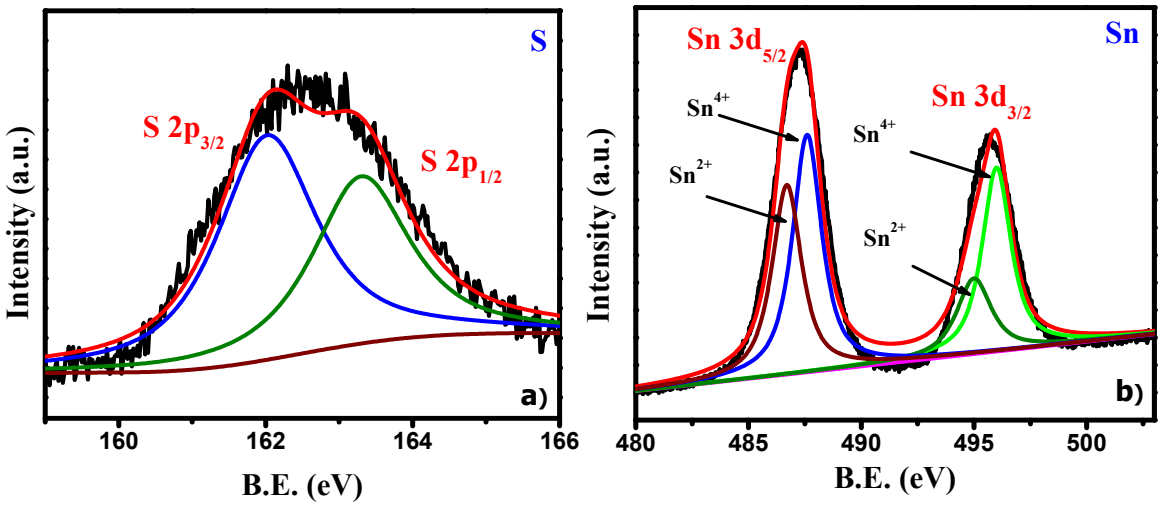

Figure S3: XPS spectra of **a)** Sulphur (S); **b)** Tin (Sn) of CTS

S4: Surface Energy Calculations

The optimized lattice parameters of the bulk phase were used for simulating the 2 × 2 surface of the Cu_3SnS_4 with full chemical stoichiometry of the material with 2 unit-cell thickness to form a slab model of it (total 64 atoms). The surface energies were estimated for both metal (Cu-Sn) and non-metal (S) terminated facet along the <001> direction. The surface energy was computed and estimated with the following formula:

$$E_s = 1/A \times (E_{slab} - N_s \times E_{bulk}) \ldots\ldots\ldots (1)$$

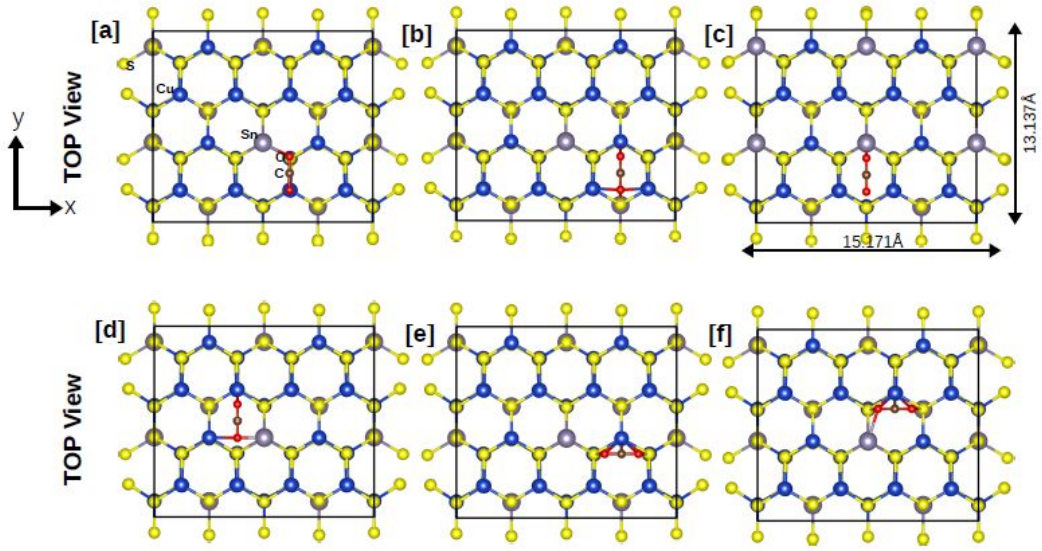

Figure S4: The models of 2 × 2 hybrid surface of CTS along <001> with CO_2 adsorbed. Cu, Sn, S, C and O atoms are marked with blue, gray, yellow, brown, and red colour balls, respectively.

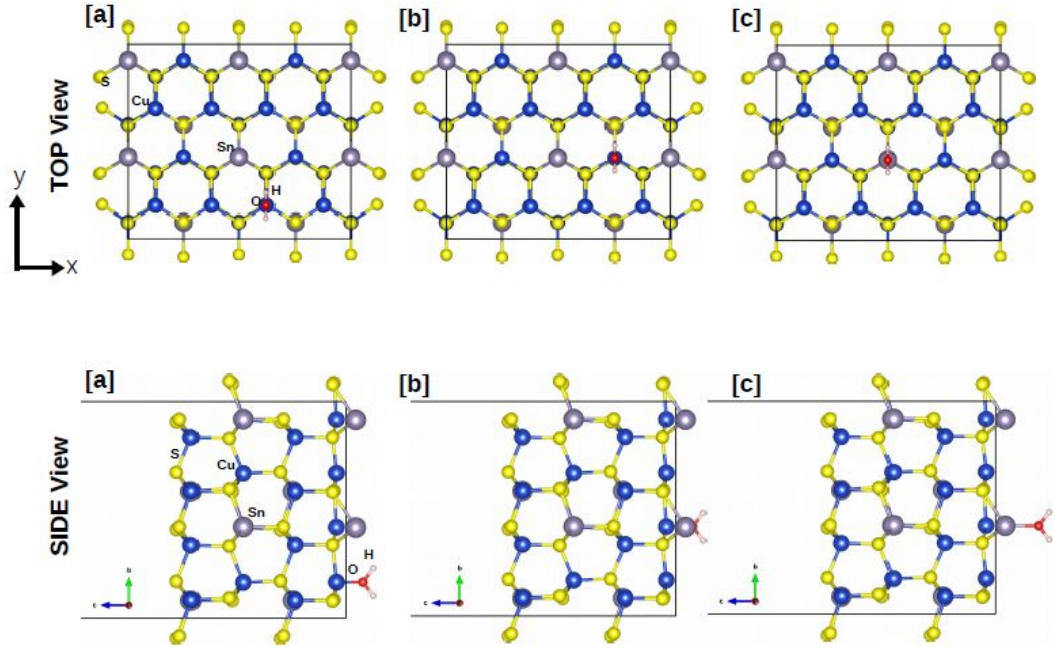

Figure S5: The models of 2 × 2 hybrid surface of CTS along <001> with H_2O adsorbed. The Cu, Sn, and S atoms are marked in the same ways like the previous with additional O and H atoms are shown in small red and white color balls.

where, E_s is calculated surface energy of the model, E_{slab} is total energy of the pristine slab, E_{bulk} is total energy per atom of the bulk Cu_3SnS_4 and N_s is total number of atoms in the slab, A is the in-plane surface area of the model pristine slab. For the slab models, the vacuum was chosen to the more than 20Å and a Monkhorst-Pack k-point mesh of size 4 × 6 × 1 grid was used for the simulation of the selective atomic positions relaxation of top two layers of 2 × 2 slab of CTS and post processing of the binding energies of CO_2 and H_2O over the metal terminated surface of it.

The details of the surface energies estimation of the CTS are given in our previous research work.[7] The nature of surface CO_2 and H_2O adsorption were checked with the PBE-GGA+D3 calculations, which includes van der Waals (vdW) dispersion energies corrections in an empirical way as implemented in D3 approach in VASP code.[8,9]

Table S1: The calculated binding energies of CO_2 and H_2O adsorption on the metal terminated surface of CTS from PBE-GGA+D3 calculations.

Models of CO_2		Models of H_2O	
Model No.	***Binding Energy, E_b (eV)***	***Model No.***	***Binding Energy, E_b (eV)***
[a]	-0.135	[a]	-0.210
[b]	-0.660	[b]	-0.220
[c]	-0.056	[c]	+0.085
[d]	-0.107		
[e]	-0.087		
[f]	-0.115		

The binding energies of the individual case of the CO_2 or H_2O were measured theoretically using the formula,

$$E_b = (E_{hy} - E_{slab} - E_{gas} + \Delta ZPE) \ldots\ldots (2)$$

where E_b, E_{hy}, E_{slab}, E_{gas} and ΔZPE are respectively the binding energy of each gas molecule, total energy of hybrid model (i.e. either CO_2 or H_2O or both attached to the surface of CTS),

total energy of the pristine slab of CTS without gas, total energy of gas molecule without slab within the model and change in zero-point energies calculated using the vibrational frequencies. The details of the all possible model of CO_2 and H_2O adsorption sites are shown in the **Figure S4 and S5**, respectively. The calculated binding energies of these models are shown in the **Table S1** calculated from PBE-GGA+D3 approach.

S5: Physisorption of Isolated H_2O Molecule over CTS Surface

All possible models those are used in our study of the H_2O adsorption over the CTS surface for PBE-GGA+D3 optimization are given in **Figure S5-S7**. Here we have shown models with the most favourable binding energy from our calculations as mentioned in the Table S1.

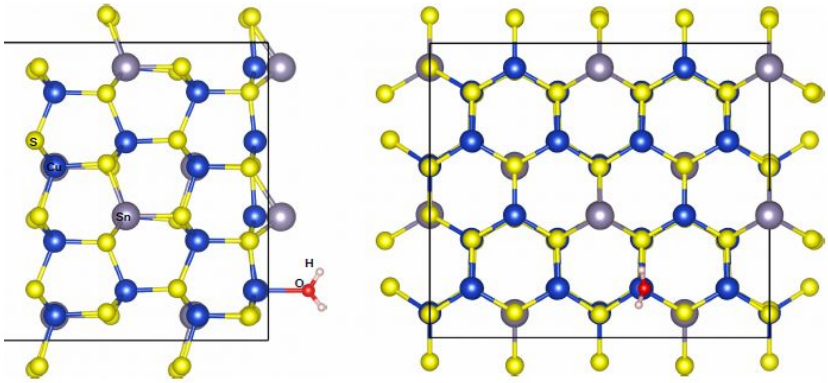

Figure S6: PBE-GGA+D3 functional optimized Model [a] as mentioned in Table S1 for H_2O

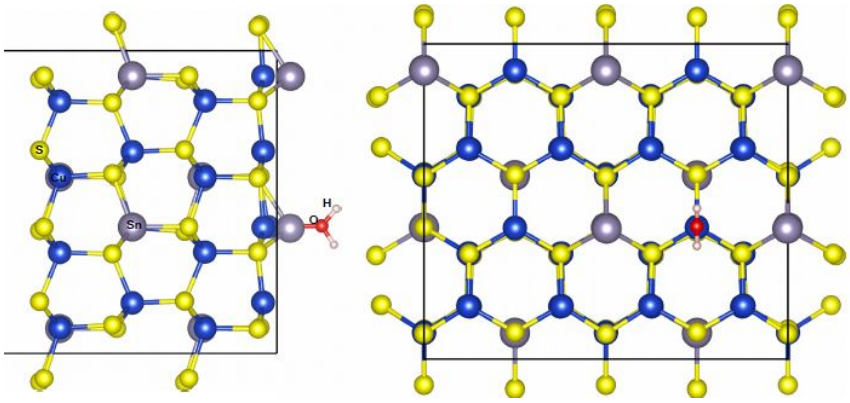

Figure S7: PBE-GGA+D3 functional optimized Model [b] as mentioned in Table S1 for H_2O

S6: Physisorption of Isolated CO_2 Molecule over CTS Surface

All possible models those are used in our study of the CO_2 adsorption over the CTS surface for PBE-GGA+D3 optimization are given in **Figure S8-S11**. Here we have shown models with the most favourable binding energy from our calculations as mentioned in the Table S1.

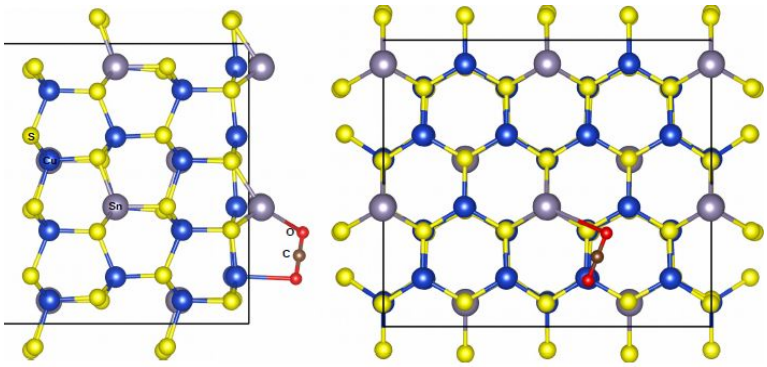

Figure S8: PBE-GGA+D3 functional optimized Model [a] as mentioned in Table S1 for CO_2

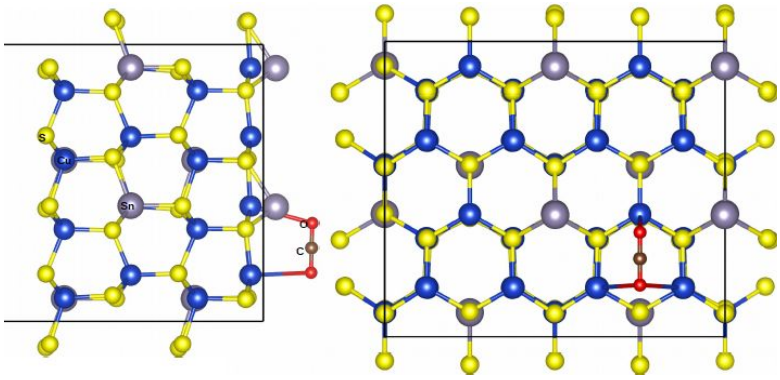

Figure S9: PBE-GGA+D3 functional optimized Model [b] as mentioned in Table S1 for CO_2

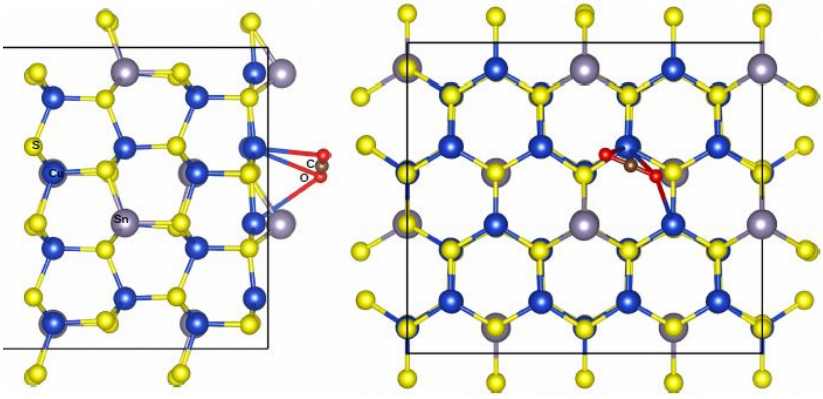

Figure S10: PBE-GGA+D3 functional optimized Model [d] as mentioned in Table S1 for CO_2.

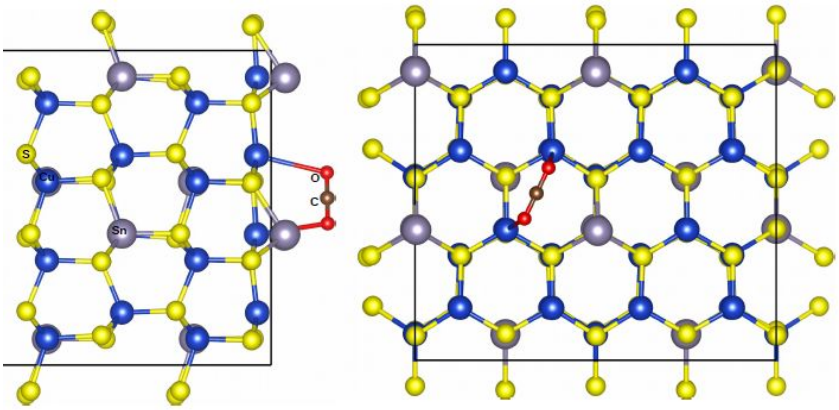

Figure S11: PBE-GGA+D3 functional optimized Model [f] as mentioned in Table S1 for CO_2.

S7: Effect of H_2O for Activation of CO_2 and Formation of $HCOO^-$

The favourable and unfavourable situation of the CO_2+H_2O models over the CTS (001) surface geometry after PBE-GGA+D3 optimization are shown below. Calculations are done over the 2×2 surface of the CTS as discussed earlier section, and only part of it projected for better visualization.

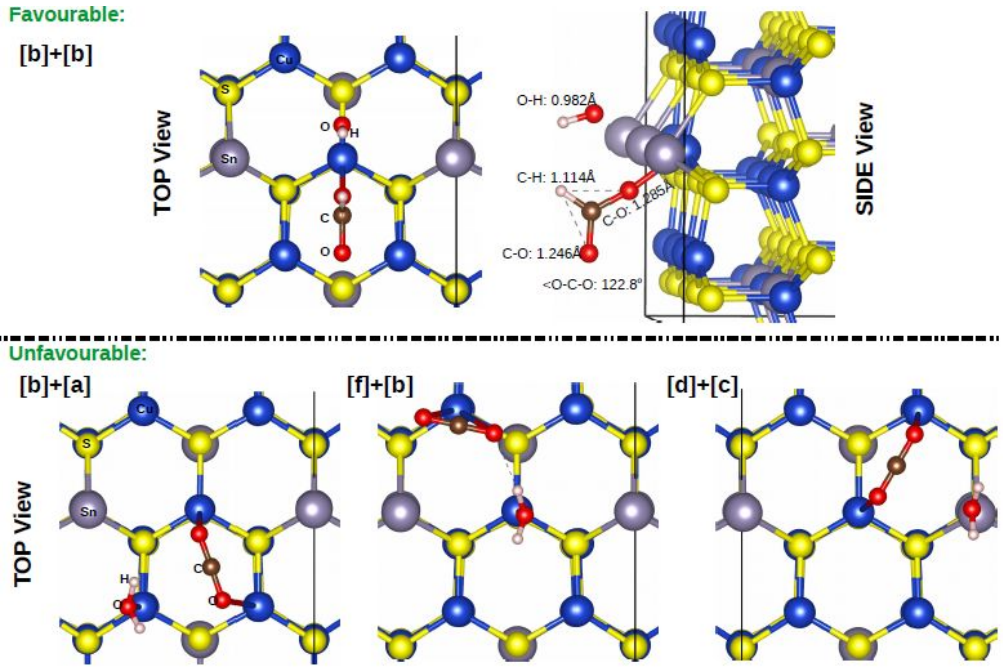

Figure S12: PBE-GGA+D3 functional optimized combined CO_2 and H_2O models for formate pathway confirmation.

S8: HER data

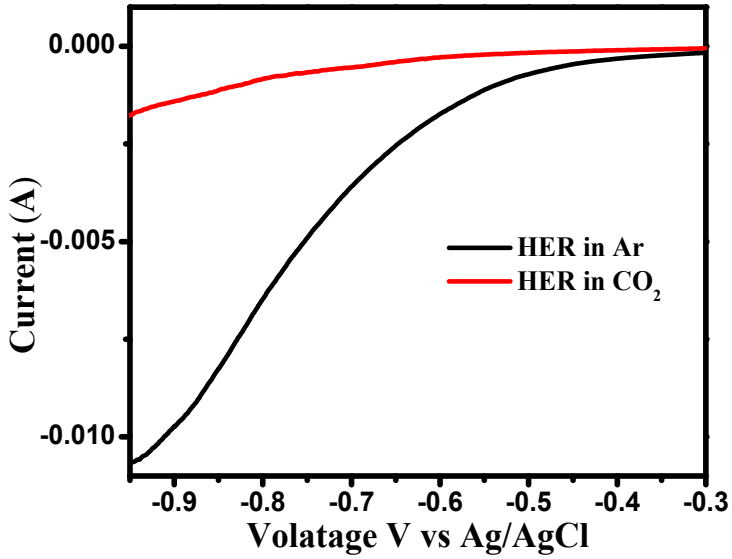

Figure S13: HER data of CTS in presence of CO_2 and Ar.

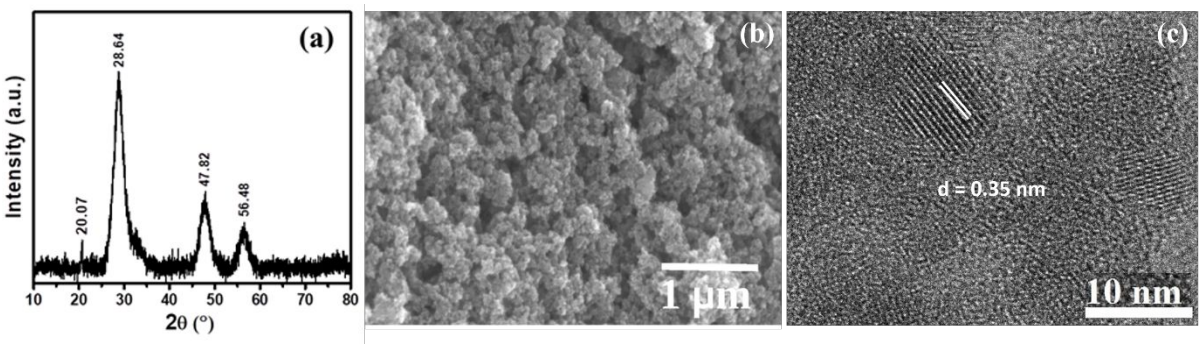

Figure S14. Physical characterization of CTS nanoparticles. (a) PXRD, (b) FESEM (Copyright Wiley-VCH Verlag GmbH & Co. KGaA, 2018. Reproduced with permission from Reference 7) and (c) TEM.

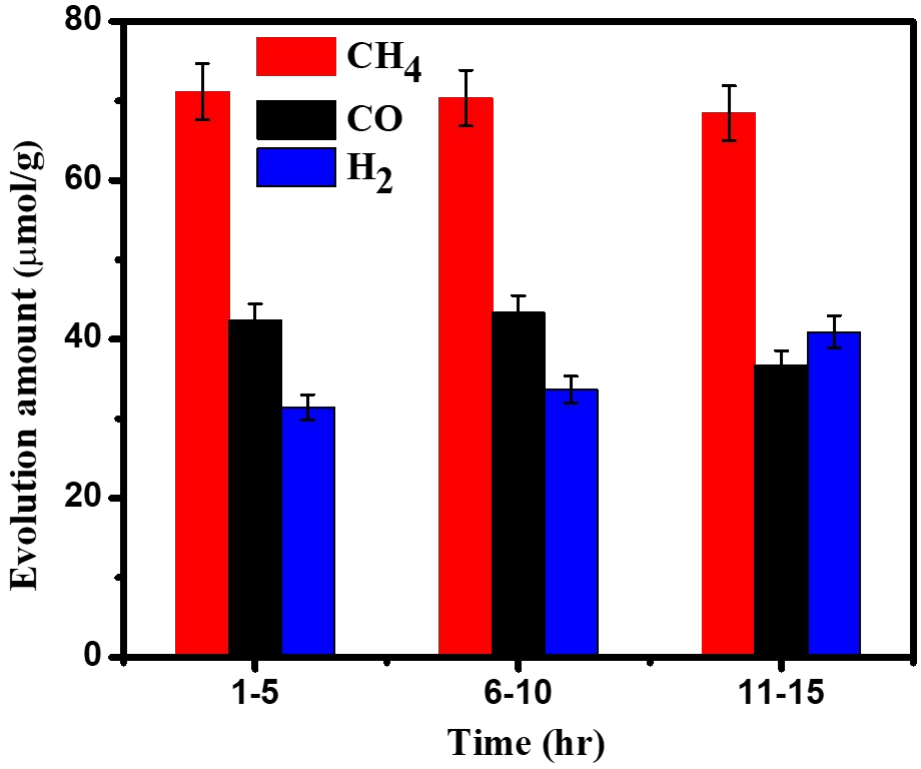

Figure S15. Histograms showing 5 hrs stability data with 3 repetitions for CH_4, CO and H_2.

Table S2: Table of Comparison of different sulphides based photocatalyst for photocatalytic CO_2 reduction

S.No.	Photocatalyst	CH_4 (µmol/g/hr)	CO (µmol/g/hr)	CH_3OH (µmol/g/hr)	Selectivity of products	Light source	Ref
1.	CdS CdS/WO_3	0.1 1.02			-	3 W LED Lamp	10
2.	CdS/ZnS	0.7	0.14		-	8 W Hg Lamp UV	11
3.	CdS/enzyme		0.6 µmol/hr*		-	250 W Tungsten-Halogen Lamp	12
4.	CdS CdS/Graphene	0.2 3	0.14 0.3		-	-	13
5.	CdS/Ni		3 µmol/hr*		90%	100 mW/cm^2	14
6.	Cd/ZnS	-	81.3		-	200 W Hg-Xe Lamp	15
7.	CdS/MOF		50.4 µmol*		50%	420 nm LED Lamp	16
8.	Bi_2S_3			20	-	300 W Xe Lamp	17
9.	Bi_2S_3 CdS Bi_2S_3/CdS			40 20 70	-	500 W Xe Lamp	18
10.	BCN BCN/CdS		30 160		85%	300 W Xe Lamp	19
11.	CdS CdS/Ag/rGO		0.3 µmol/hr* 1.5 µmol/hr*		38%	300 W Xe Lamp	20
12.	CdS CdS/rGO	0.21 2.51			-	3 W LED Lamp	21
13.	TiO_2 $CuInS_2/TiO_2$	1.25 2.5		0.7 0.86	-	350 W Xe Lamp	22
14.	**CTS**	**14**	**8.5**		**80%**	**300 W Xe lamp**	**This Work**

*mg of catalyst not available.

References

(1) Kresse, G.; Hafner, J. Ab Initio Molecular Dynamics for Liquid Metals. *Phys. Rev. B* **1993**, *47* (1), 558–561.

(2) Kresse, G.; Furthmüller, J. Efficient Iterative Schemes for Ab Initio Total-Energy Calculations Using a Plane-Wave Basis Set. *Phys. Rev. B* **1996**, *54* (16), 11169–11186.

(3) Kresse, G.; Joubert, D. From Ultrasoft Pseudopotentials to the Projector Augmented-Wave Method. *Phys. Rev. B* **1999**, *59* (3), 1758–1775.

(4) Perdew, J. P.; Burke, K.; Ernzerhof, M. Generalized Gradient Approximation Made Simple. *Phys. Rev. Lett.* **1996**, *77* (18), 3865–3868.

(5) Heyd, J.; Scuseria, G. E.; Ernzerhof, M. Hybrid Functionals Based on a Screened Coulomb Potential. *J. Chem. Phys.* **2003**, *118* (18), 8207–8215.

(6) Blaha, P.; Schwarz, K.; Madsen, G. K. H.; Kvasnicka, D.; Luitz, J. *{WIEN2K}, {A}n {A}ugmented {P}lane {W}ave + {L}ocal {O}rbitals {P}rogram for {C}alculating {C}rystal {P}roperties*; {K}arlheinz Schwarz, Techn. Universität Wien, Austria, 2001.

(7) M, T.; Sharma, N.; Das, T.; Varhade, S.; Badadhe, S. S.; Thotiyl, M. O.; Kabir, M.; Ogale, S. A Combined Experimental and Computational Study of Gas Sensing by Cu_3SnS_4 Nanoparticulate Film: High Selectivity, Stability, and Reversibility for Room Temperature H_2S Sensing. *Adv. Mater. Interfaces* **2018**, *5* (10), 1701492–1701500.

(8) Grimme, S.; Ehrlich, S.; Goerigk, L. Effect of the Damping Function in Dispersion Corrected Density Functional Theory. *J. Comput. Chem.* **2011**, *32* (7), 1456–1465.

(9) Grimme, S.; Antony, J.; Ehrlich, S.; Krieg, H. A Consistent and Accurate Ab Initio Parametrization of Density Functional Dispersion Correction (DFT-D) for the 94 Elements H-Pu. *J. Chem. Phys.* **2010**, *132* (15), 154104.

(10) Jin, J.; Yu, J.; Guo, D.; Cui, C.; Ho, W. A Hierarchical Z-Scheme CdS-WO_3 Photocatalyst with Enhanced CO_2 Reduction Activity. *Small* **2015**, *11* (39), 5262–5271.

(11) Kočí, K.; Praus, P.; Edelmannová, M.; Ambrožová, N.; Troppová, I.; Fridrichová, D.; Słowik, G.; Ryczkowski, J. Photocatalytic Reduction of CO_2 Over CdS, ZnS and Core/Shell CdS/ZnS Nanoparticles Deposited on Montmorillonite. *J. Nanosci. Nanotechnol.* **2017**, *17* (6), 4041–4047.

(12) Chaudhary, Y. S.; Woolerton, T. W.; Allen, C. S.; Warner, J. H.; Pierce, E.; Ragsdale, S. W.; Armstrong, F. A. Visible Light-Driven CO_2 reduction by Enzyme Coupled CdS Nanocrystals. *Chem. Commun.* **2012**, *48* (1), 58–60.

(13) Cho, K. M.; Kim, K. H.; Park, K.; Kim, C.; Kim, S.; Al-Saggaf, A.; Gereige, I.; Jung, H. T. Amine-Functionalized Graphene/CdS Composite for Photocatalytic Reduction of CO_2. *ACS Catal.* **2017**, *7* (10), 7064–7069.

(14) Kuehnel, M. F.; Orchard, K. L.; Dalle, K. E.; Reisner, E. Selective Photocatalytic CO_2 Reduction in Water through Anchoring of a Molecular Ni Catalyst on CdS Nanocrystals. *J. Am. Chem. Soc.* **2017**, *139* (21), 7217–7223.

(15) Meng, X.; Yu, Q.; Liu, G.; Shi, L.; Zhao, G.; Liu, H.; Li, P.; Chang, K.; Kako, T.; Ye, J. Efficient Photocatalytic CO_2 Reduction in All-Inorganic Aqueous Environment: Cooperation between Reaction Medium and Cd(II) Modified Colloidal ZnS. *Nano Energy* **2017**, *34* (Ii), 524–532.

(16) Wang, S.; Wang, X. Photocatalytic CO_2 reduction by CdS Promoted with a Zeolitic Imidazolate Framework. *Appl. Catal. B Environ.* **2015**, *162*, 494–500.

(17) Jin, J.; He, T. Facile Synthesis of Bi_2S_3 Nanoribbons for Photocatalytic Reduction of CO_2 into CH_3OH. *Appl. Surf. Sci.* **2017**, *394*, 364–370.

(18) Li, X.; Chen, J.; Li, H.; Li, J.; Xu, Y.; Liu, Y.; Zhou, J. Photoreduction of CO_2 to Methanol over Bi_2S_3/CdS Photocatalyst under Visible Light Irradiation. *J. Nat. Gas Chem.* **2011**, *20* (4), 413–417.

(19) Zhou, M.; Wang, S.; Yang, P.; Huang, C.; Wang, X. Boron Carbon Nitride Semiconductors Decorated with CdS Nanoparticles for Photocatalytic Reduction of CO_2. *ACS Catal.* **2018**, *8* (6), 4928–4936.

(20) Zhu, Z.; Han, Y.; Chen, C.; Ding, Z.; Long, J.; Hou, Y. Reduced Graphene Oxide-Cadmium Sulfide Nanorods Decorated with Silver Nanoparticles for Efficient Photocatalytic Reduction Carbon Dioxide Under Visible Light. *ChemCatChem* **2018**, *10* (7), 1627–1634.

(21) Yu, J.; Jin, J.; Cheng, B.; Jaroniec, M. A Noble Metal-Free Reduced Graphene Oxide-CdS Nanorod Composite for the Enhanced Visible-Light Photocatalytic Reduction of CO_2 to Solar Fuel. *J. Mater. Chem. A* **2014**, *2* (10), 3407–3416.